A Low Mach Preconditioned Harmonic Balance Solver for Cavity Flutter Computations

Pierre Sivel[1]
Institute of Propulsion Technology,
German Aerospace Center (DLR),
Linder Höhe, 51147 Cologne, Germany
email: pierre.sivel@dlr.de

Christian Frey
Institute of Propulsion Technology,
German Aerospace Center (DLR),
Linder Höhe, 51147 Cologne, Germany
email: christian.frey@dlr.de

Hans-Peter Kersken
Institute of Propulsion Technology,
German Aerospace Center (DLR),
Linder Höhe, 51147 Cologne, Germany
email: hans-peter.kersken@dlr.de

Edmund Kügeler
Institute of Propulsion Technology,
German Aerospace Center (DLR),
Linder Höhe, 51147 Cologne, Germany
email: edmund.kuegeler@dlr.de

Labyrinth seal flutter is a critical phenomenon in turbomachinery, as it can lead to severe structural vibrations and potential component damage. Accurate prediction and mitigation of flutter are paramount to ensuring the reliability and performance of modern turbomachinery systems. This paper explores the numerical computation of a labyrinth seal flutter test case using a low Mach preconditioned harmonic Balance (HB) solver and investigates how this approach can improve the accuracy and response time of flutter computations.

HB solvers have gained prominence in turbomachinery computations for their ability to efficiently capture unsteady flow phenomena and significantly reduce computational time compared to time-domain analyses. In labyrinth seals, however, the flow is often characterized by low Mach numbers, and preconditioning for these conditions has been shown to significantly improve convergence and accuracy. The goal of this paper is to demonstrate how to implement low Mach preconditioning in a HB solver in the frequency domain.

We employ iterative preconditioning to alleviate the stiffness associated with density-based solvers under low Mach conditions and analyze the effect of the preconditioning parameters on the convergence rate. Furthermore, we address inaccuracies linked to the classical Roe solver in low Mach scenarios by adapting it to the low Mach preconditioned governing equations. Through the combined utilization of iterative preconditioning and a preconditioned Roe solver, this study aims to improve convergence rates and the overall quality of flutter predictions.

We demonstrate the method with an academic labyrinth seal test case originally presented by Corral et al. [1]. While previous investigations have primarily relied on linearized frequency domain solvers and reduce-order models, in this research a preconditioned HB solver is applied to this test case.

Keywords: Harmonic Balance, Low Mach Preconditioning, Labyrinth Seal Flutter

1 Introduction

Controlling leakage flow in turbomachinery is crucial for optimizing the machine's performance. Labyrinth seals limit leakage flow between rotating and non-rotating components by dissipating kinetic energy through a series of fins and cavities [2]. These seals, however, are susceptible to aeroelastic instabilities, which can lead to structural damage and critical engine failure [3]. Therefore, it is essential to make precise and reliable predictions of the aeroelastic stability of labyrinth seals.

Alford [4] investigated aeroelastic instabilities in labyrinth seals, emphasizing the significance of the support side and the tangential velocity in reducing self-excited vibrations. Ehrich [5] highlighted the sensitivity of seal stability to the fin clearance, and derived the first analytical model for seal flutter predictions. Abbott [6] pointed out that, in addition to the support side, the ratio of the acoustic frequency to the seal's natural frequency determined its stability and developed an analytical model based on these two criteria.

With advances in modern numerical methods, computational fluid dynamics (CFD) has become a viable tool for comprehensive aeroelastic stability analysis of labyrinth seals. Hirano et al. [7] used a steady-state solver to compute rotor dynamic forces in a five-finned straight labyrinth seal. They found that analytical models produced pessimistic predictions of the forces within the seal. Phibel et al. [8], Di Mare et al. [9] and, more recently, Miura and Sakai [10] conducted comprehensive stability analysis of realistic four finned labyrinth seals, identifying relevant parameters and methods to suppress seal flutter. Miura and Sakai [10] confirmed their results and demonstrated good agreement with experimental data. These studies demonstrate the potential of using CFD to improve our understanding of labyrinth seal flutter. However, unsteady time-domain CFD simulations require considerable computational resources.

In recent years, Corral and Vega [11, 12], proposed a model to predict flutter in labyrinth seals, based on an analytical formulation of the work per cycle inside the cavity. To validate this model, Greco and Corral [13] computed an academic two-finned labyrinth seal using a linearized frequency-domain CFD solver. Linearized computations are an efficient alternative to unsteady-time domain simulations. However, they are limited to small displacement amplitudes to avoid nonlinear effects.

HB solvers [14, 15] are an efficient approach to reduce the cost of non-linear unsteady CFD computations. Here, the temporal periodicity is used to express the solution in terms of truncated Fourier series about the system's fundamental frequency. This yields a non-linear system of equations for the solution's harmonics, that can be solved directly in the frequency domain with efficient steady-state methods. This significantly reduces the computational cost compared to conventional unsteady time-domain methods.

However, an additional challenge in the computation of labyrinth seals is the low Mach numbers that dominate the flow within the seal's cavities. In density-based solvers, low Mach numbers tend to cause degraded convergence rates and inaccurate solutions [16–18]. both problems can be overcome using low Mach preconditioning techniques.

[1]Corresponding Author.

The slow convergence at low Mach numbers results from the discrepancy between the acoustic and convective timescales. To equalize the timescales of the system, iterative preconditioning artificially reduces the acoustic speed in the pseudo-time. this method was first introduced by Chorin [19] for incompressible solvers and later adapted for steady-state compressible solvers by Turkel [16]. Used in combination with a dual-time stepping scheme, it preserves temporal accuracy in unsteady computations. However, Venkateswaran and Merkle [20] found that for unsteady simulations, the optimal preconditioning parameter depends on the physical time step size. They proposed a new preconditioner for unsteady time-domain simulations. This method has since been applied by Campobasso and Baba-Ahmadi [21] and Djeddi et al. [18] in a HB solver, which solves the HB system of equations in the time-domain.

The standard Roe scheme [22], produces excessive dissipation at low Mach numbers, leading to inaccurate solutions [23]. To address this issue, Godfrey et al. [24] proposed an adapted version of the Roe scheme, known as the preconditioned Roe scheme (P-Roe). In P-Roe, the artificial dissipation is derived based on the preconditioned convective fluxes and retrieves the proper dissipation for convective low Mach flows. However, Potsdam et al. [25] showed, that using P-Roe excessively dampens acoustic waves and is therefore not suitable for unsteady computations. Potsdam et al. [25] proposed an adaptation of the preconditioned Roe dissipation, which blends the preconditioned dissipation based on a steady preconditioner [16] and an unsteady preconditioner [20]. This method achieves proper dissipation for convective flows, while maintaining good accuracy for acoustic waves.

The main goal of this paper is to present an accurate and efficient low Mach preconditioned HB solver for labyrinth seal flutter predictions. To achieve this goal, we convert the time step dependency of the unsteady preconditioner by Venkateswaran and Merkle [20] into a dependency of the system's frequency. We apply the iterative preconditioner to the two-finned academic labyrinth seal presented by Greco and Corral [13] and perform a parameter analysis to optimize the preconditioning parameters. Additionally, the results for two academic test cases are reported: the steady lid driven cavity and an acoustic wave propagation test case. These results demonstrate the shortcomings of the classical Roe scheme and P-Roe schemes compared to Potsdam's Roe scheme. Finally, a stability analysis of the labyrinth seal is performed using the HB solver with iterative preconditioning in combination with Potsdam's Roe scheme.

2 Harmonic Balance

The unsteady governing equations are defined as

$$\frac{\partial q}{\partial t} + R\left(q\right) = 0 \tag{1}$$

where, t represents the physical time, q represents the state vector and R represents the nonlinear residual. For time-periodic solutions, the state is expressed in terms of Fourier series about the frequency ω

$$q\left(t,x,y,z\right) = \mathrm{Re}\left(\sum_{k=0}^{\infty} \widehat{q}_k\left(x,y,z\right) e^{ik\omega t}\right). \tag{2}$$

Here, $\hat{q}_k$ is the Fourier coefficient of the k-th harmonic of ω. The state is approximated by a finite number of harmonics K and is inserted in the governing Equations (1), leading to the nonlinear HB system of equations

$$ik\omega\widehat{q}_k + \widehat{R}_k(q) = 0, \quad \text{for} \quad k = 0,\dots,K. \tag{3}$$

Because the time-domain residual R is nonlinear, its Fourier coefficients $\widehat{R}_k(q)$ depend on all harmonics of the state $\widehat{q}_k$. To solve the system of equations, we use a mixed frequency-domain time-domain method. In each iteration, the state is reconstructed at equidistant sampling points in time. Then at each sampling point, the nonlinear residual is computed and the harmonics of the residual are computed using of a Fourier transform. The system of Equations (3) is solved in the frequency domain using pseudo-time marching [26].

3 Low Mach Preconditioning

3.1 Iterative Preconditioning. The main goal of iterative preconditioning is to improve the convergence of low Mach simulations by artificially reducing the acoustic velocity to the same order as the local convective velocity. This is achieved by multiplying the time derivative of the governing equations with the preconditioning matrix P^{-1}, which alters the characteristics of the computed system [16]. For the steady-state governing equations solved using a pseudo-time marching scheme, the preconditioned equations are

$$P^{-1}\frac{\partial q}{\partial \tau} + R\left(q\right) = 0 \tag{4}$$

where τ is the pseudo-time. In this work, we use the preconditioning matrix proposed by Turkel [27]. In conservative variables it is defined as

$$P^{-1} = I + \frac{\left(\frac{1}{\beta^2}-1\right)(\gamma-1)}{a^2}$$
$$\begin{pmatrix} \|U\|^2 - E & -u & -v & -w & 1 \\ u\left(\|U\|^2 - E\right) & -u^2 & -vu & -wu & u \\ v\left(\|U\|^2 - E\right) & -uv & -v^2 & -wv & v \\ w\left(\|U\|^2 - E\right) & -uw & -vw & -w^2 & w \\ H\left(\|U\|^2 - E\right) & -uH & -vH & -wH & H \end{pmatrix}. \tag{5}$$

Here, I is the identity matrix, a is the speed of sound, γ is the specific heat ratio, $U = (u, v, w)$ is the vector of cartesian velocity components, H is the specific total enthalpy and E is the specific total energy [27]. the preconditioner is controlled by the preconditioning parameter β^2. The appropriate definition of β^2 is crucial to guarantee an efficient but stable computation. For steady computations, it is defined as

$$\beta^2 = \min\left(1, \max\left(k_\beta M^2, \frac{\Delta p}{\rho a^2}, \left(\frac{\nu}{a\Delta h}\right)^2, \beta^2_{\min}\right)\right) \tag{6}$$

where M is the local Mach number, Δp is the maximum pressure difference between neighboring cells, ν is the dynamic viscosity and Δh is a characteristic cell length. This definition consists of the following terms:

- $k_\beta M^2$: Definition for the optimal equalization of the timescales [16]. $k_\beta \geq 1$ is a stabilization parameter.
- $\left(\frac{\nu}{a\Delta h}\right)^2$: Equalization of the acoustic and diffusive timescales for very low Reynolds numbers [28].
- $\frac{\Delta p}{\rho a^2}$: Stabilization for large local pressure fluctuations [29].
- $\beta^2_{\min}$: User-defined lower limit, to avoid singular preconditioning matrix [16].

For $\beta^2 = 1$, the preconditioning matrix becomes the identity matrix and the non-preconditioned system is retrieved. The preconditioner is disabled in the supersonic regime by ensuring $\beta^2 \leq 1$. In the

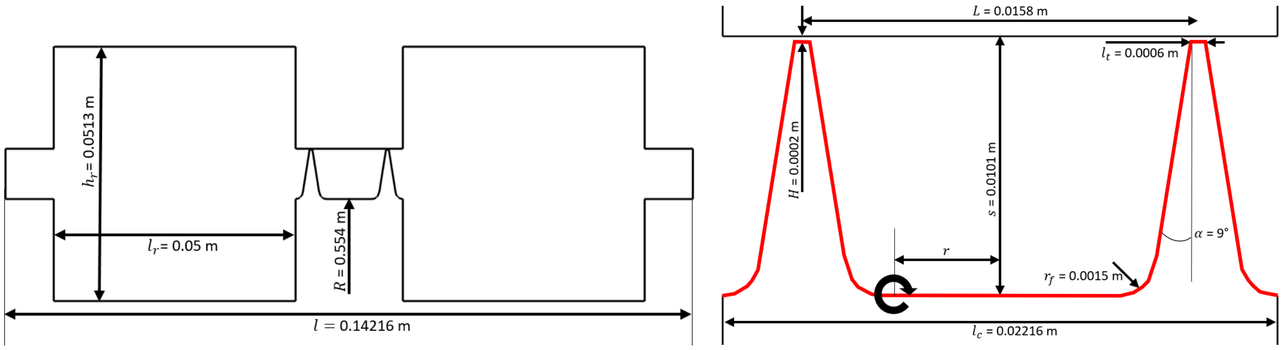

Fig. 1 2D representation of the academic two-finned labyrinth seal test case with measurements

following sections, the definition in Eq. (6) of the preconditioning parameter will be called "steady preconditioning".

In unsteady time-domain computations, a dual-time stepping scheme is used to prevent the loss of temporal accuracy caused by preconditioning

$$P^{-1}\frac{\partial q}{\partial \tau}+\frac{\partial q}{\partial t}+R\left(q\right)=0. \tag{7}$$

For very large physical time steps Δt, the steady preconditioner greatly improves the convergence of the pseudo-time iterations. However, for very small physical time steps Δt, the non-preconditioned system already converges optimally and steady preconditioning tends to worsen the convergence [20]. Therefore, Venkateswaran and Merkle [20] introduced an unsteady Mach number M_{u}^2 as an additional lower limit for the preconditioning parameter

$$\beta_{\mathrm{u}}^2=\min\left(1,\max\left(k_\beta M^2,\frac{\Delta p}{\rho a^2},\left(\frac{\nu}{a\Delta h}\right)^2,\beta_{\min}^2,M_{\mathrm{u}}^2\right)\right), \tag{8}$$

with

$$M_{\mathrm{u}}^2=\left(\frac{L}{\pi\Delta t a}\right)^2. \tag{9}$$

Here, the time step Δt represents the largest resolved frequency and L is a characteristic length of the computation, which represents the largest resolved wave length. L is typically set to the size of the computational domain [20, 25].

In this paper, we apply iterative preconditioning to the HB equations analogously to Eq. (7)

$$P_k^{-1}\frac{\partial \widehat{q}_k}{\partial \tau}+ik\omega\widehat{q}_k+\widehat{R}_k(q)=0,\quad \text{for}\quad k=0,\ldots,K. \tag{10}$$

For the HB system, the frequencies of the solution are part of the problem setup. It is thus natural to replace the definition of the unsteady Mach number in Eq. (9) with

$$M_{\mathrm{hb},k}^2=\left(\frac{L\omega_k}{2\pi^2 a}\right)^2 \tag{11}$$

where ω_k is a frequency defined in the following. Then, the preconditioning parameter and the preconditioning matrix P_k are computed according to Eq. (8).

As for the definition of ω_k, we differentiate between two types of preconditioning. The first setup employs a single definition for the unsteady Mach number (cf. Eq. (11)) for all harmonics and will be called "unsteady preconditioning" below. Here, $M_{\mathrm{hb},k}^2$ is based on the frequency of the first harmonic, i.e., $\omega_k=\omega$. The second setup ("individual preconditioning") uses an individual unsteady Mach number (cf. Eq. (11)) for each harmonic, i.e., $\omega_k=k\omega$. In particular, the mean flow is preconditioned with the steady preconditioning.

It should be noted, that, since iterative preconditioning alters the pseudo-time characteristics of the computed system, boundary conditions that are formulated in terms of characteristics need to be adjusted. The non-reflecting boundary conditions used in the following computations are formulated in the frequency domain. The boundary conditions for each harmonic employ the preconditioned characteristic matrix for the corresponding preconditioning parameter [30].

3.2 Preconditioned Dissipation. The artificial dissipation of the standard Roe scheme [22] is

$$F_{\mathrm{d,Roe}}=-\frac{1}{2}|\widetilde{D}|\Delta q \tag{12}$$

where $D=\frac{\partial F}{\partial q}+\frac{\partial G}{\partial q}+\frac{\partial H}{\partial q}$, F, G and H are the convective fluxes in each cartesian direction and Δq denotes the difference between the left and right face states. The tilde denotes quantities based on the Roe-averaged state [22]. The Roe matrix $|\tilde{D}|$ is computed based on the eigenvectors R and the absolute values of the eigenvalues λ_{i} of the flux Jacobian $\tilde{D}$

$$|\widetilde{D}|=R|\Lambda|R^{-1} \tag{13}$$

where R is the right eigenvector matrix and $|\Lambda|=\mathrm{diag}\left(|\lambda_1|,|\lambda_2|,|\lambda_3|,|\lambda_4|,|\lambda_5|\right)$.

At low Mach numbers, the classical Roe scheme exhibits poor scaling of the artificial dissipation resulting in inaccurate prediction of convective flows [23]. A commonly used approach to retrieve proper scaling is to redefine the Roe matrix based on the low Mach preconditioned convective fluxes [24, 31]. This yields the so-called P-Roe scheme with the artificial dissipation

$$F_{\mathrm{d,P\text{-}Roe}}=-\frac{1}{2}\widetilde{P}^{-1}|\widetilde{P}\widetilde{D}|\Delta q. \tag{14}$$

Although this method is derived from iterative preconditioning, it can be used independently [31]. Therefore, when using P-Roe, we will always apply the steady preconditioning parameter (cf. Eq. (6)) for the corrected dissipation in Eq. (14) regardless of whether unsteady, individual, or no preconditioning is applied for the iterative preconditioning.

P-Roe does greatly improve the accuracy of convective low Mach simulations, but in unsteady computations, it excessively dampens acoustic waves [21]. To maintain the accuracy of P-Roe, while simultaneously reducing the damping of acoustic waves, Potsdam et al. [25] proposed a novel Roe scheme, which blends the preconditioned dissipation based on the steady preconditioner (cf. Eq. (6)) with the preconditioned dissipation based on the unsteady

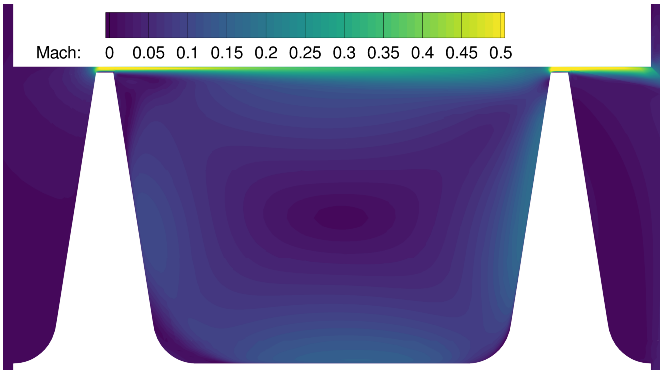

Fig. 2 Mean distribution of the Mach number inside the labyrinth seal

preconditioner in Eq. (8). Here, the definition of the unsteady Mach number in Eq. (9) is used based on the frequency of the first harmonic. The resulting artificial dissipation reads

$$F_{\mathrm{d,Potsdam}} = -\frac{1}{2}\widetilde{P}_{\mathrm{u}}^{-1}\left(|\widetilde{P}_{\mathrm{u}}\widetilde{D}|L_{\mathrm{u}} + |\widetilde{P}_{\mathrm{s}}\widetilde{D}|L_{\mathrm{s}}\right)\Delta q. \quad (15)$$

The subscripts u and s described the use of the steady and unsteady preconditioners respectively and $L_{\mathrm{u/s}}$ are the blending matrices, which are described in the appendix.

4 Test Case

This study applies the low Mach preconditioned HB solver to the academic two-finned straight labyrinth seal, which was investigated by Greco and Corral [13] using a linearized frequency domain solver. Figure 1 presents the test case's geometry along with all relevant measurements. The original publications [1, 13] provided the cavity radius, the cavity height, the seal clearance and the inter-fin distance. Missing geometrical parameters were extracted from the illustrations in those publications and might differ slightly from the original test case.

Figure 2 depicts the Mach number distribution within the seal's inter-fin cavity. Mach numbers up to 0.65 are observed at the seal's fin clearance, while the Mach number is 0.001 in the corners of the cavity. To ensure uniform pressure at the inlet and outlet of the seal, two large relaxation chambers are positioned at each end of the seal [13]. In these chambers, the Mach number does not exceed 0.005 and 0.05 in the inlet and outlet chambers, respectively, which poses a major challenge for classical density-based solvers. Therefore, this test case is ideal to test the capabilities of the low Mach preconditioned HB solver.

The computations are performed using the HB solver of the hybrid finite volume multi-block solver TRACE [15], developed at the German Aerospace Center (DLR). The iterative preconditioning techniques used in these computations were presented in section 3.1. The convective fluxes are discretized using one of the Roe schemes presented in section 3.2, which are elevated to second-order accuracy using the MUSCL reconstruction [32]. The viscous fluxes are discretized using a central scheme. The turbulence is modeled using the log-ω Menter-SST turbulence model [33] in combination with the Kato Launder stagnation point anomaly fix [34]. Higher harmonics of the turbulent quantities resolving the unsteadiness of turbulence are not included in the computations. Transitional effects are neglected, therefore, no transition model is used. An implicit Euler backward pseudo-time marching scheme is employed to solve both the steady and HB equations. The local pseudo-time step is calculated for each cell and each harmonic based on the local solution and the iterative preconditioning parameter, using a CFL number of 10 for all simulations.

The entire computational grid is composed of 291 680 cells, with 10 cells in pitch-wise direction, resolving a pitch segment of 10°. Without the relaxation chambers, the mesh for the labyrinth seal comprises 137 800 cells. The domain is periodic in pitch-wise direction. All wall boundary layers are resolved with $y^+ < 1$, using a low-Reynolds no-slip boundary condition. The inlet and outlet interfaces of the domain are modeled using low Mach preconditioned non-reflecting boundary conditions (NRBC) [30]. At the inlet, the stagnation temperature and the pressure, as well as the flow angles are prescribed, whereas at the outlet, the static pressure is prescribed. The pressure ratio of the seal is $\pi_{\mathrm{T}} = p_{\mathrm{t,\,inlet}}/p_{\mathrm{outlet}} = 1.5$ and the Reynolds number based on the fin clearance and the inlet velocity is Re = 25 320. All HB computations are initialized with a steady-state solution.

For the flutter analysis, torsion modes are prescribed on the bottom wall of the seal (depicted in red in Fig. 1). The torsion center is positioned at the same radius as the bottom of the inter-fin cavity, at three different axial positions, $r = -0.069$ m, $r = 0.0087$ m and $r = 0.122$ m (see Fig. 1). For each torsion radius, the prescribed torsion amplitude is adapted to ensure a maximum displacement at the fin tip of 0.1% of the fin clearance. The unsteady flow generated by the motion of the seal is resolved with only one harmonic, since nonlinear effects are not expected at these amplitudes. Five equidistant sampling points in time are used for the reconstruction of the HB system's non-linear residual.

For the iterative preconditioning and the preconditioned dissipation, the lower limit of the preconditioning parameter is $\beta^2_{\mathrm{min}} = 10^{-20}$ and the stabilization parameter is $k_\beta = 10$. The characteristic length L is given for each computation in the following section.

5 Iterative Preconditioning

The labyrinth seal test case is computed without preconditioning, with the steady preconditioner, with the unsteady preconditioner and with the individual preconditioner. In a first step, to isolate the effect of the iterative preconditioner, the classical Roe scheme is applied for the artificial dissipation. The results presented in this section focus on the torsion mode with the frequency $f = 423.6$ Hz, which matches the non-dimensional frequency from the computations performed by Greco and Corral [13]. The nodal diameter is set to ND = 6 and the torsion radius to $r = 0.0087$ m. The convergence of other nodal diameters and torsion radii was similar. For the unsteady and individual preconditioners, the characteristic length is $L = 0.142$ m, which corresponds to the length of the domain in axial direction.

Figure 3 compares the convergence history of the L1-residuals of the zeroth and first harmonics for each preconditioner. For the zeroth harmonic, the individual and the steady preconditioners yield the fastest computations, reaching a converged state after approximately 80 000 iterations. The unsteady preconditioner and the non-preconditioned computations did not reach a fully converged state after 200 000 iterations. However, the final residual using the unsteady preconditioner is three orders of magnitude smaller than the non-preconditioned residual. For the first harmonic, the non-preconditioned computation yields by far the fastest convergence, reaching a reduction of the initial residual by seven orders of magnitude in 200 000 iterations. The steady preconditioner resulted in the worst convergence, reducing the residual by only two orders of magnitude over 200 000 iterations. The individual and unsteady preconditioners yield the exact same convergence, showing only a slightly improved convergence rate compared to the steady preconditioner. Even though the individual preconditioner does not yield the overall fastest convergence for both harmonics, these results demonstrate that, indeed, it does combine the behavior of the steady preconditioner for the zeroth harmonic and the unsteady preconditioner for the first harmonic.

To find a better setup for the convergence of the individual preconditioner in the first harmonic, a parameter analysis for the characteristic length is performed. The resulting convergence history of the residual of the first harmonic is depicted in Fig. 4(*a*). Increasing L and, therefore, $M^2_{\mathrm{hb},1}$ continuously improves the convergence

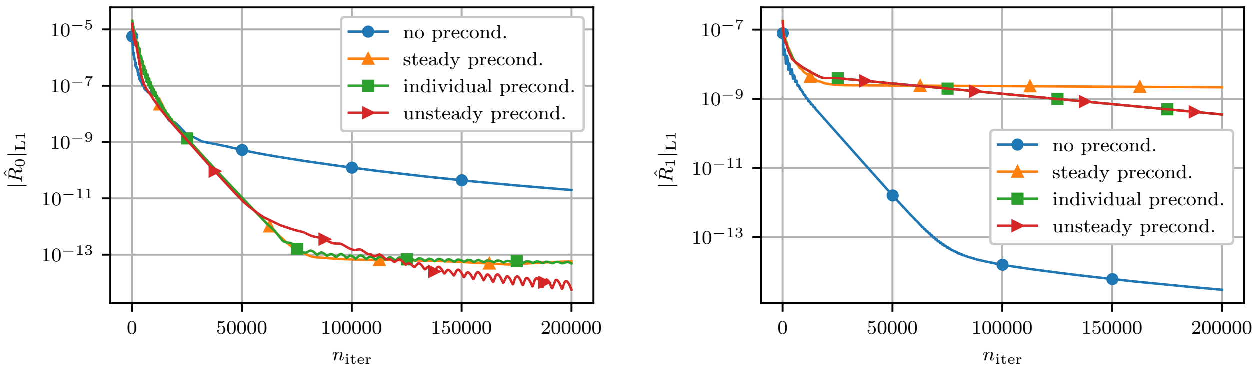

(*a*) 0th harmonic

(*b*) 1st harmonic

Fig. 3 Convergence history of the L1-residuals of the harmonics for f = 423.6 Hz, r = 0.0087 m and ND = 6, with L = 0.142 m ($M^2_{\mathrm{hb},1} \approx 1e-3$)

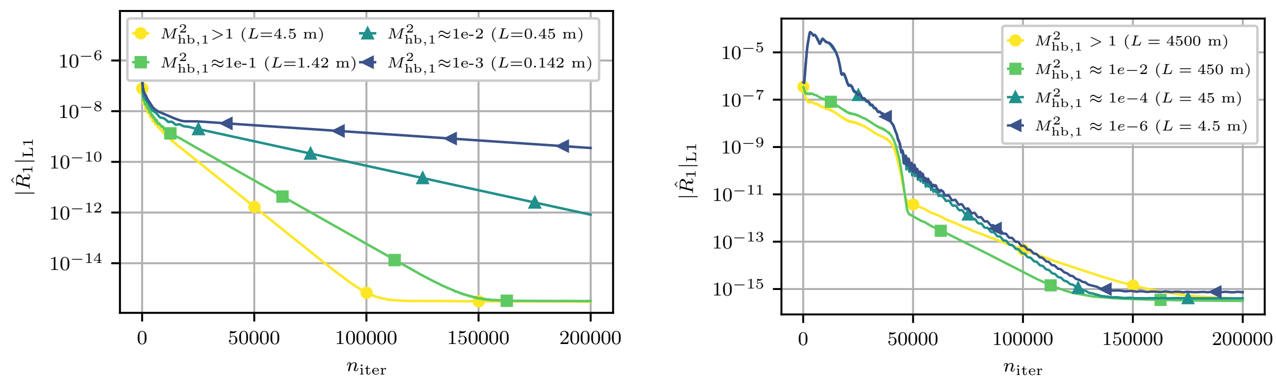

(*a*) f = 423.6 Hz

(*b*) f = 1.2 Hz

Fig. 4 Convergence History of the L1-residuals of the first harmonic using individual preconditioning for r = 0.0087 m and ND = 6 for varying L

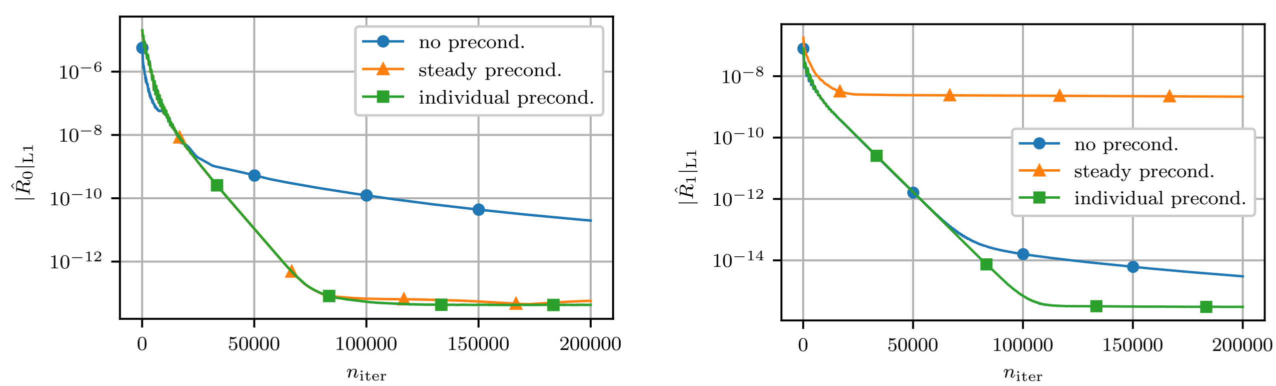

(*a*) 0th-harmonic

(*b*) 1st-harmonic

Fig. 5 Convergence History of the L1-residuals of the harmonics for f = 423.6 Hz, r = 0.0087 m and ND = 6, with L = 4.5 m ($M^2_{\mathrm{hb},1}$ = 1).

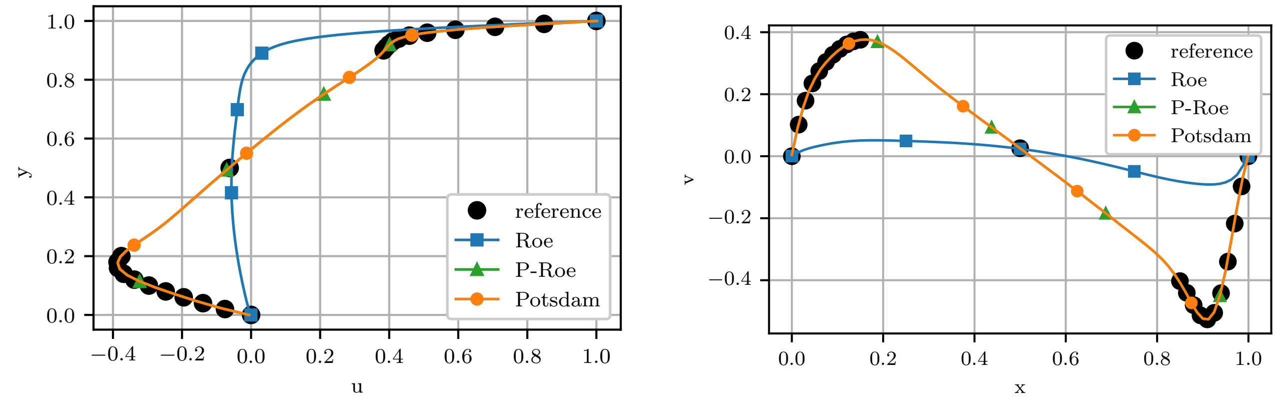

(*a*) Vertical velocity profile

(*b*) Horizontal velocity profile

Fig. 6 Velocity profiles through the center of the lid driven cavity for Re = 1000

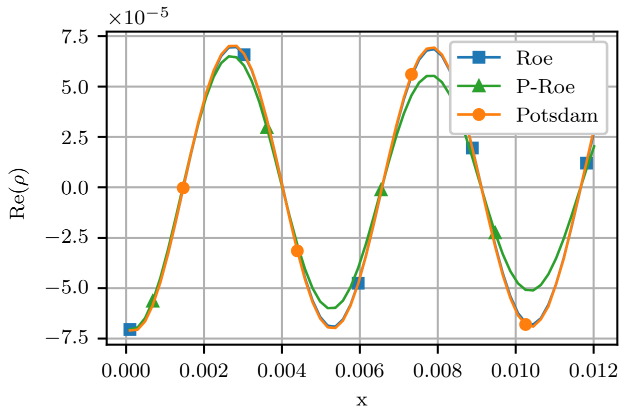

Fig. 7 Real part of the density of an acoustic wave with an amplitude of 10 Pa at M = 0.01.

rate of the simulation, until $M^2_{\mathrm{hb},1} = 1$ is reached and the preconditioner is disabled. At this point, the convergence rate is at its highest. This means that for this specific frequency, any form of preconditioning for the first harmonic will harm the convergence.

One might suspect that preconditioning the first harmonic will always have a negative impact on its convergence. Therefore, the same parameter study as above is performed for a significantly lower frequency of $f = 1.2\,\mathrm{Hz}$ and the results are presented in Fig. 4(*b*). For the small frequency, all L leading to $M^2_{\mathrm{hb},1} < 1$ yield a faster convergence than not preconditioning the first harmonic at all ($M^2_{\mathrm{hb},1} > 1$). This means that deactivating the preconditioner is not always the optimal approach for the higher harmonics. Furthermore, the results for the two frequencies indicate that a much greater value for L than the domain length is necessary to improve the convergence.

Figure 5 compares the convergence history of simulations using the individual preconditioner, the steady preconditioner and the non-preconditioned with a value of $L = 4.5\,\mathrm{m}$, effectively deactivating the preconditioning of the first harmonic. Compared to the previous runs, adapting the individual preconditioner for the first harmonic did not influence the convergence of the zeroth harmonic. However, even though both the non-preconditioned computation and the individual preconditioner have the same preconditioning parameters, with the individual preconditioner, the first harmonic reaches a converged state after approximately 120 000 iterations. Supposedly, the improved convergence of the zeroth harmonic contributes to a faster convergence of the first harmonic. In contrast, the non-preconditioned computation requires approximately 1 000 000 iterations to fully converge both harmonics to machine precision. Therefore, the individual preconditioner reduces the number of iterations by approximately 88%.

6 Preconditioned Dissipation

Before applying P-Roe and Potsdam's Roe scheme to the labyrinth seal test case, the shortcomings of the classical Roe scheme and P-Roe are demonstrated using two additional academic test cases. For the computation of the academic test case, the iterative preconditioner is deactivated to isolate the effect of the artificial dissipation on the computations.

The first test case is the steady-state lid driven cavity, which consists of a 2D squared domain enclosed in four solid walls. The upper wall of the domain moves at a constant speed of $u_{\mathrm{wall}} = 1\,\mathrm{m/s}$, driving the flow inside the cavity. This simplified labyrinth seal cavity imitates the vortex structure inside labyrinth seal cavities. With a domain length of $l = 0.014\,81\,\mathrm{m}$, the initial conditions are defined, such that a Reynolds number based on the wall velocity of 1000 is attained. The Mach number in the domain ranges between $M = 10^{-3}$ and 10^{-8}. The test case is computed with the standard Roe scheme, the P-Roe scheme and with Potsdam's blended Roe scheme. Since this is a steady state computation, the unsteady Mach number for Potsdam's scheme is set to $M^2_{\mathrm{hb},1} = 1$. The simulations are performed on a 81x81 grid, and the results are compared with the reference computed by Erturk [35] on a 601x601 grid using an incompressible solver.

The x-velocity and y-velocity profiles along $x = l/2$ and $y = l/2$, respectively, are presented in Fig. 6 for each artificial dissipation. The standard Roe scheme fails to predict the correct strength and position of the vortex inside the cavity, leading to a strong disparity to the reference. P-Roe and Potsdam's scheme are both in very good agreement with the reference. This demonstrates that the two adapted dissipation formulations should be preferred over the standard Roe scheme to accurately predict low-speed convective flows in labyrinth seal cavities.

Next, an inviscid acoustic wave propagation test case is computed with the HB solver. The domain is 0.0125 m long and periodic in y-direction. At the entry of the domain, an acoustic wave is prescribed with a frequency of 78 531.4 Hz and an amplitude of 10 Pa. The domain is discretized by a 64x64 grid. The background mach number is 0.01. For Potsdam's scheme L is set to the domain length.

Figure 7 shows the real part of the density of the acoustic wave propagating through the domain. The Roe scheme and Potsdam's scheme both yield similar results, with a reduction of the wave

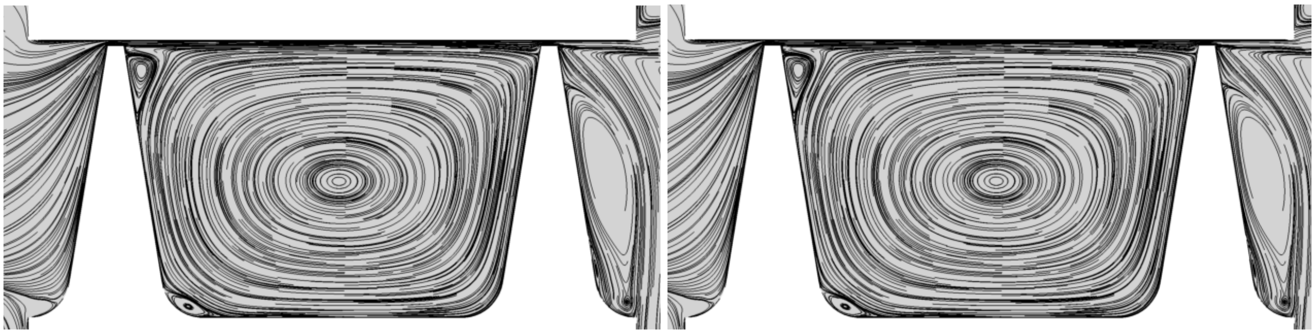

(*a*) non-preconditioned (*b*) preconditioned

Fig. 8 Streamlines of the zeroth harmonic inside the inter-fin cavity for f = 423.6 Hz, r = 0.0087 m and ND = 6

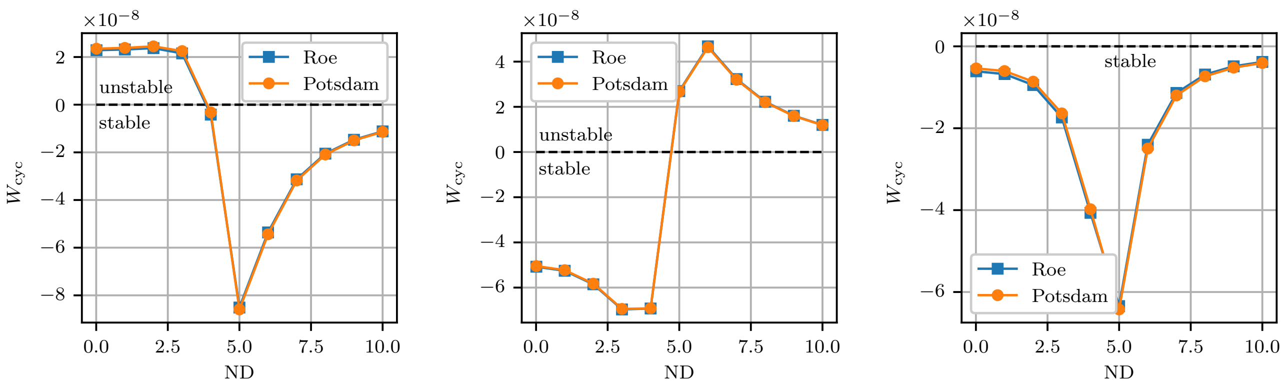

(*a*) r = −0.069 m (*b*) r = 0.0087 m (*c*) r = 0.122 m

Fig. 9 Work per cycle over the nodal diameter for three different locations of the torsion center for f = 423.6 Hz

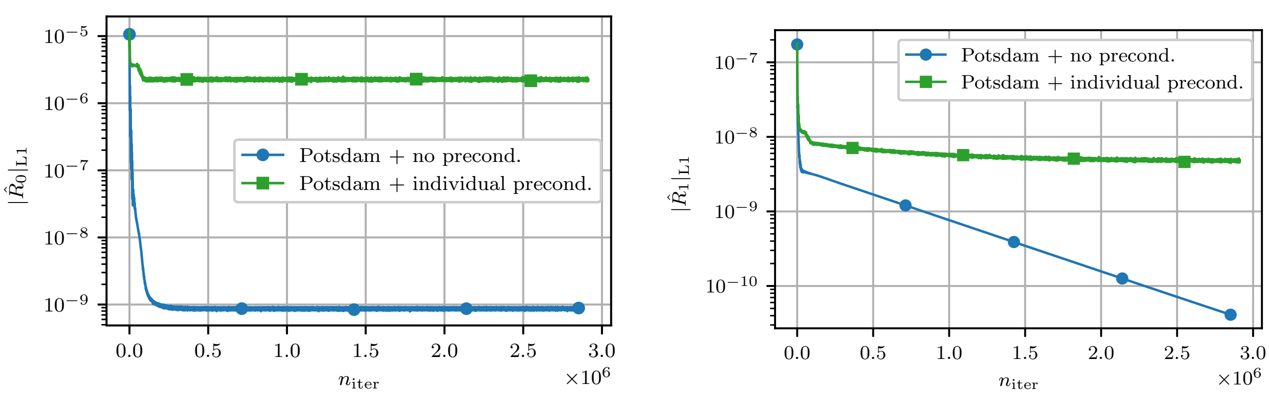

(*a*) 0th harmonic (*b*) 1st harmonic

Fig. 10 Comparison of the convergence History of the L1-norm of the residuals for Potsdam's scheme with and without iterative preconditioning with f = 423.6 Hz, r = 0.0087 m and ND = 6

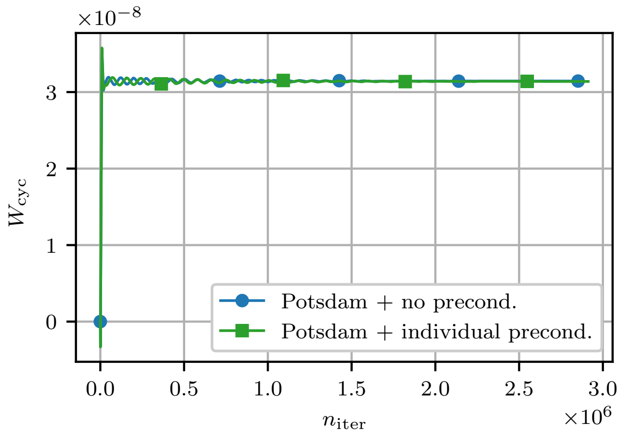

Fig. 11 Convergence history of the work per cycle for f = 423.6 Hz, r = 0.0087 m and ND = 6 using Potsdam's scheme with and without iterative preconditioning

amplitude by 6.3 % over the domain length. P-Roe, however, attenuates the acoustic wave significantly more, resulting in a reduction of the amplitude by 31.2 %, demonstrating the limited applicability of P-Roe for unsteady computations.

We infer from the results of the academic test cases that, out of the three presented schemes, only Potsdam's scheme is able to accurately predict both convective and acoustic effects in the low Mach regime. Therefore, for the stability analysis of the labyrinth seal, we only compare Potsdam's scheme with the original classical Roe. For this analysis, we apply the optimized individual preconditioner with $M^2_{\mathrm{hb},1} = 1$ for the first harmonic and steady preconditioning for the zeroth harmonic, as described in section 5. $M^2_{\mathrm{hb},1} = 1$ is chosen for Potsdam's scheme to be consistent with the iterative preconditioner. The stability analysis is performed for the constant torsion frequency of $f = 423.6$ Hz, nodal diameters 0 to 10 and the three torsion radii: $r = -0.069$ m, $r = 0.0087$ m and $r = 0.122$ m. These parameters correspond to a seal supported on the high-pressure side, on the low-pressure side close to the cavity center, and on the low-pressure side far from the cavity center, respectively.

Figure 8 depicts the streamlines of the mean flow on a 2D-slice at a constant pitch angle of 0° for $r = 0.0087$ m and ND = 6. The overall structure of the flow inside the cavity is very similar for Roe and for Potsdam's scheme. However, the vortices forming in the corners and at the entry of the cavity are predicted to be larger when Potsdam's scheme is used. The improvement of the solution is not as significant as for the lid driven cavity test case, which may result from the Mach number in the labyrinth seal being several orders of magnitude larger. Still, it should be noted that the discrepancies between the two solutions are most dominant where the Mach number is the smallest (see Fig. 2).

In Figure 9, we compare the predicted work per cycle computed with both methods and the resulting seal stability predictions for all three torsion radii. The results predicted by both schemes are in good agreement with the literature [1, 13]. The seal supported far on the low-pressure side (cf. Fig. 9(*c*)) is predicted to be stable for all nodal diameters. However, when the torsion center is close to the cavity center on the low-pressure side (cf. Fig. 9(*b*)), it becomes unstable at large nodal diameters. If the seal is supported on the high-pressure side (cf. Fig. 9(*a*)), it remains stable for large nodal diameter and becomes unstable for small nodal diameters. Overall, Potsdam's scheme does not change the predicted stability compared with the standard Roe scheme. For the torsion center close to the cavity center at $r = 0.0087$ m, the work per cycle is consistent between both schemes, only varying by 0.1% to 1%. The discrepancy in the computed work per cycle increases with increasing torsion radius. At $r = 0.069$ m and $r = 0.122$ m, results computed using Potsdam's scheme deviate from the Roe scheme's prediction by 1.7% to 11%.

Figure 10 presents the convergence history of the labyrinth seal computations using Potsdam's scheme with and without individual preconditioning for $f = 423.6$ Hz, $r = 0.0087$ m and ND = 6. Comparing the convergence of the labyrinth seal computed with Potsdam's scheme and with Roe scheme (cf. Fig. 3) showcases that the improved accuracy of Potsdam's scheme comes at the cost of a reduced convergence level and convergence rate. Further, the originally optimized individual preconditioner does not yield a faster convergence than the non-preconditioned case anymore when used in combination with Potsdam's scheme. It should be noted that, even though the computations do not converge down to machine precision, the convergence of the work per cycle is quite satisfactory (cf. Fig. 11).

The two academic test cases indicate that Potsdam's scheme should be used to ensure high-quality HB computations. Additional analysis of the iterative preconditioner combined with preconditioned dissipation will be necessary to improve the convergence while guaranteeing the best possible accuracy of the HB solver at low Mach numbers.

7 Conclusions

This paper has presented the implementation of low Mach preconditioning techniques for HB solvers, combining iterative preconditioning and preconditioning of the artificial dissipation. The methods were applied and optimized on an academic labyrinth seal flutter test case. The main results of this study were:

- Optimal convergence requires individual preconditioning for each harmonic. Special attention must be paid to the unsteady Mach number $M^2_{\mathrm{hb},1}$, since choosing an ill-suited value can hinder convergence.
- The classical Roe scheme is inadequate for convective low Mach flows, while P-Roe excessively attenuates acoustic waves. To ensure accurate HB computations in the low Mach regime, it is recommended to use Potsdam's Roe scheme.
- The combination of iterative preconditioning with Potsdam's scheme unexpectedly hinders the convergence. This indicates the need for further optimization of the preconditioner with respect to this particular combination.

These conclusions highlight the potential of low Mach preconditioning techniques to improve both the quality of the solution and to reduce the computational cost of labyrinth seal flutter analysis using HB solvers. Moving forward, future research should delve deeper into the optimization of the combination of iterative preconditioning with Potsdam's Roe scheme.

Nomenclature

a = Speed of sound (m s^{-1})
D = Convective flux Jacobian (-)
E, F, G = Convective flux Jacobian in cartesian directions (-)
E = Specific total energy (J kg^{-1})
f = frequency (s^{-1})
F_{d} = Artificial dissipation vector (-)
h_{r} = Relaxation chamber height (m)
H = Fin cleanrance (m)
H = Specific total enthalpy (J kg^{-1})
I = Identity matrix (-)
k_{β} = Stabilization constant (-)
l = Computational domain length (m)
l_{c} = Cavity length (m)
l_{r} = Relaxation chamber length (m)
l_{t} = Fin tip width (m)
L = Inter-fin distance (m)

$L_{u/s}$ = Blending matrix (Potsdam) (-)
L = Characteristic Length (m)
M = Mach number (-)
M_{u} = Unsteady Mach number (time-domain) (-)
M_{hb} = Unsteady Mach number (harmonic balance) (-)
ND = Nodal diameter (-)
p = Static pressure (Pa)
p_{t} = Stagnation pressure (Pa)
P = Preconditioning matrix (-)
q = State vector (-)
$\widehat{q}$ = Fourier coefficient of the state vector (-)
r = Torsion radius (m)
r_{f} = Fillet radius (m)
R = Nonlinear time domain residual (-)
R = Cavity radius (m)
$\widehat{R}$ = Fourier coefficient of the residual (-)
Re = Reynolds number (-)
s = Cavity height (m)
t = Physical time (s)
U = Velocity vector (m s^{-1})
u, v, w = Cartesian velocities (m s^{-1})
x, y, z = Cartesian coordinates (m)
y^+ = non-dimensional cell size in normal direction (-)

Greek Letters

α = Fin wall angle (°)
β^2 = Preconditioning parameter (-)
β^2_{min} = Lower limit for the preconditioning parameter (-)
γ = Isentropic heat ratio (-)
π_{T} = Pressure ratio (-)
λ_{i} = Convective flux eigenvalue (m s^{-1})
Λ = Convective flux eigenvalue matrix (m s^{-1})
ν = Kinematic viscosity (m s^{-2})
ρ = Density (kg m^{3})
τ = Pseudo-time (s)
ω = Angular frequency (rad s^{-1})

Superscripts and Subscripts

$\tilde{}$ = Roe-averaged
HB = Harmonic balance
k = k-th harmonic
s = Steady
u = Unsteady

Appendix A: POTSDAM'S BLENDING MATRICES

The goal of the blending matrices is to apply the artificial dissipation either only on the pressure field or on the velocity and temperature field. Therefore, in primitive temperature variables $q_T = (p, u, v, w, T)$, the matrices are

$$L_{\mathrm{u}} = \mathrm{diag}\,(1, 0, 0, 0, 0) \tag{A1}$$

and

$$L_{\mathrm{s}} = \mathrm{diag}\,(0, 1, 1, 1, 1)\,. \tag{A2}$$

Since the implementation of the Roe scheme is in conservative variables $q = (\rho, \rho u, \rho v, \rho w, \rho E)$, they can be transformed to conservative variables via

$$L_{\mathrm{u/s,cons}} = \frac{\partial q}{\partial q_T} L_{u/s} \frac{\partial q_T}{\partial q}. \tag{A3}$$

This results in the following conservative matrices:

$$L_{\mathrm{u,cons}} = \begin{pmatrix} a_1+1 & a_2 & a_3 & a_4 & a_5 \\ a_1 u & a_2 u + 1 & a_3 u & a_4 u & a_5 u \\ a_1 v & a_2 v & a_3 v + 1 & a_4 v & a_5 v \\ a_1 w & a_2 w & a_3 w & a_4 w + 1 & a_5 w \\ a_1 H & a_2 H & a_3 H & a_4 H & a_5 H + 1 \end{pmatrix}, \tag{A4}$$

and

$$L_{\mathrm{s,cons}} = \begin{pmatrix} -a_1+1 & -a_2 & -a_3 & -a_4 & -a_5 \\ -a_1 u & -a_2 u + 1 & -a_3 u & -a_4 u & -a_5 u \\ -a_1 v & -a_2 v & -a_3 v + 1 & -a_4 v & -a_5 v \\ -a_1 w & -a_2 w & -a_3 w & -a_4 w + 1 & -a_5 w \\ -a_1 H & -a_2 H & -a_3 H & -a_4 H & -a_5 H + 1 \end{pmatrix}, \tag{A5}$$

with the parameters

$$a_1 = \frac{\gamma}{2a^2} (\gamma - 1) \left(u^2 + v^2 + w^2\right) \tag{A6}$$

$$a_2 = -\frac{\gamma}{2a^2} (\gamma - 1)\, u \tag{A7}$$

$$a_3 = -\frac{\gamma}{2a^2} (\gamma - 1)\, v \tag{A8}$$

$$a_4 = -\frac{\gamma}{2a^2} (\gamma - 1)\, w \tag{A9}$$

$$a_5 = \frac{\gamma}{2a^2} (\gamma - 1)\,. \tag{A10}$$

References

[1] Corral, R., Greco, M., and Vega, A., 2021, "Higher Order Conceptual Model for Labyrinth Seal Flutter," Journal of Turbomachinery, **143**(7).
[2] Chupp, R. E., Hendricks, R. C., Lattime, S. B., and Steinmetz, B. M., 2006, "Sealing in Turbomachinery," NASA.
[3] Lewis, D., Platt, C., and Smith, E., 1978, "Aeroelastic Instability in F100 Labyrinth Air Seals," *14th Joint Propulsion Conference*, American Institute of Aeronautics and Astronautics, doi: 10.2514/6.1978-1087.
[4] Alford, J. S., 1964, "Protection of Labyrinth Seals From Flexural Vibration," Journal of Engineering for Power, **86**(2), pp. 141–147.
[5] Ehrich, F., 1968, "Aeroelastic Instability in Labyrinth Seals," Journal of Engineering for Power, **90**(4), pp. 369–374.
[6] Abbott, D. R., 1981, "Advances in Labyrinth Seal Aeroelastic Instability Prediction and Prevention," Journal of Engineering for Power, **103**(2), pp. 308–312.
[7] Hirano, T., Guo, Z., and Kirk, R. G., 2003, "Application of CFD Analysis for Rotating Machinery: Part 2 - Labyrinth Seal Analysis," *Proceedings of the ASME Turbo Expo 2003*, ASMEDC, doi: 10.1115/gt2003-38984.
[8] Phibel, R., di Mare, L., Green, J. S., and Imregun, M., 2009, "Numerical Investigation of Labyrinth Seal Aeroelastic Stability," *Proceedings of the ASME Turbo Expo 2009*, ASMEDC, doi: 10.1115/gt2009-60017.
[9] Di Mare, L., Imregun, M., Green, J. S., and Sayma, A. I., 2010, "A Numerical Study of Labyrinth Seal Flutter," Journal of Tribology, **132**(2).
[10] Miura, T. and Sakai, N., 2019, "Numerical and Experimental Studies of Labyrinth Seal Aeroelastic Instability," Journal of Engineering for Gas Turbines and Power, **141**(11).
[11] Corral, R. and Vega, A., 2018, "Conceptual Flutter Analysis of Labyrinth Seals Using Analytical Models-Part I: Theoretical Support," Journal of Turbomachinery, **140**(12).
[12] Vega, A. and Corral, R., 2018, "Conceptual Flutter Analysis of Labyrinth Seals Using Analytical Models-Part II: Physical Interpretation," Journal of Turbomachinery, **140**(12).
[13] Greco, M. and Corral, R., 2021, "Numerical Validation of an Analytical Seal Flutter Model," Journal of the Global Power and Propulsion Society, **5**, pp. 191–201.
[14] Hall, K. C., Thomas, J. P., and Clark, W. S., 2002, "Computation of Unsteady Nonlinear Flows in Cascades Using a Harmonic Balance Technique," AIAA Journal, **40**(5), pp. 879–886.
[15] Frey, C., Ashcroft, G., Kersken, H.-P., and Schlüß, D., 2019, "Flutter Analysis of a Transonic Steam Turbine Blade with Frequency and Time-Domain Solvers," International Journal of Turbomachinery, Propulsion and Power, **4**(2), p. 15.
[16] Turkel, E., 1999, "Preconditioning Techniques in Computational Fluid Dynamics," Annual Review of Fluid Mechanics, **31**(1), pp. 385–416.

[17] Howison, J. and Ekici, K., 2013, “Unsteady Analysis of Wind Turbine Flows Using the Harmonic Balance Method,” *51st AIAA Aerospace Sciences Meeting including the New Horizons Forum and Aerospace Exposition*, American Institute of Aeronautics and Astronautics, doi: 10.2514/6.2013-1107.

[18] Djeddi, R., Howison, J., and Ekici, K., 2016, “A Fully Coupled Turbulent Low-Speed Preconditioner for Harmonic Balance Applications,” Aerospace Science and Technology, **53**, pp. 22–37.

[19] Chorin, A. J., 1967, “A Numerical Method for Solving Incompressible Viscous Flow Problems,” Journal of Computational Physics, **2**(1), pp. 12–26.

[20] Venkateswaran, S. and Merkle, C., 1995, “Dual Time-Stepping and Preconditioning for Unsteady Computations,” *33rd Aerospace Sciences Meeting and Exhibit*, American Institute of Aeronautics and Astronautics, doi: 10.2514/6.1995-78.

[21] Campobasso, M. S. and Baba-Ahmadi, M. H., 2012, “Analysis of Unsteady Flows Past Horizontal Axis Wind Turbine Airfoils Based on Harmonic Balance Compressible Navier-Stokes Equations With Low-Speed Preconditioning,” Journal of Turbomachinery, **134**(6).

[22] Roe, P. L., 1981, “Approximate Riemann Solvers, Parameter Vectors, and Difference Schemes,” Journal of Computational Physics, **43**(2), pp. 357–372.

[23] Hope-Collins, J. and di Mare, L., 2023, “Artificial Diffusion for Convective and Acoustic Low Mach Number Flows I: Analysis of the Modified Equations, and Application to Roe-Type Schemes,” Journal of Computational Physics, **475**, p. 111858.

[24] Godfrey, A., Walters, R., and van Leer, B., 1993, “Preconditioning for the Navier-Stokes Equations with Finite-Rate Chemistry,” *31st Aerospace Sciences Meeting*, American Institute of Aeronautics and Astronautics, doi: 10.2514/6.1993-535.

[25] Potsdam, M., Sankaran, V., and Pandya, S., 2007, “Unsteady Low Mach Preconditioning with Application to Rotorcraft Flows,” doi: 10.2514/6.2007-4473.

[26] Frey, C., Ashcroft, G., Kersken, H.-P., and Voigt, C., 2014, “A Harmonic Balance Technique for Multistage Turbomachinery Applications,” *Proceedings of the ASME Turbo Expo 2014*, Paper No. 45615, p. V02BT39A005.

[27] Turkel, E., 1987, “Preconditioned Methods for Solving the Incompressible and Low Speed Compressible Equations,” Journal of Computational Physics, **72**(2), pp. 277–298.

[28] Weiss, J. M. and Smith, W. A., 1995, “Preconditioning Applied to Variable and Constant Density Flows,” AIAA Journal, **33**(11), pp. 2050–2057.

[29] Darmofal, D. and Siu, K., 1999, “A Robust Multigrid Algorithm for the Euler Equations with Local Preconditioning and Semi-coarsening,” Journal of Computational Physics, **151**(2), pp. 728–756.

[30] Sivel, P. and Frey, C., 2022, “Low Mach Preconditioned Non-Reflecting Boundary Conditions for the Harmonic Balance Solver,” *8th European Congress on Computational Methods in Applied Sciences and Engineering*, CIMNE, doi: 10.23967/eccomas.2022.170.

[31] Viozat, C., 1997, “Implicit Upwind Schemes for Low Mach Number Compressible Flows,” INRIA, Tech. Rep. RR-3084.

[32] van Leer, B., 1979, “Towards the Ultimate Conservative Difference Scheme. V. A Second-Order Sequel to Godunovś Method,” Journal of Computational Physics, **32**(1), pp. 101–136.

[33] Müller, M., Kersken, H.-P., and Frey, C., 2022, “A Log-w Turbulence Model Formulation for Flutter Analysis with Harmonic Balance,” *16th International Symposium on Unsteady Aerodynamics, Aeroacoustics & Aeroelasticity of Turbomachines (ISUAAAT16)*.

[34] Kato, M., 1993, “The Modeling of Turbulent Flow Around Stationary and Vibrating Square Cylinders,” *9th Symposium on Turbulent Shear Flows*.

[35] Erturk, E., 2009, “Discussions on Driven Cavity Flow,” International Journal for Numerical Methods in Fluids, **60**(3), pp. 275–294.

List of Figures

1 2D representation of the academic two-finned labyrinth seal test case with measurements . . . 3
2 Mean distribution of the Mach number inside the labyrinth seal . . . 4
3 Convergence history of the L1-residuals of the harmonics for f = 423.6 Hz, r = 0.0087 m and ND = 6, with L = 0.142 m ($M^2_{\mathrm{hb},1} \approx 1e-3$) . . . 5
(*a*) 0th harmonic . . . 5
(*b*) 1st harmonic . . . 5
4 Convergence History of the L1-residuals of the first harmonic using individual preconditioning for r = 0.0087 m and ND = 6 for varying L . . . 5
(*a*) f = 423.6 Hz . . . 5
(*b*) f = 1.2 Hz . . . 5
5 Convergence History of the L1-residuals of the harmonics for f = 423.6 Hz, r = 0.0087 m and ND = 6, with L = 4.5 m ($M^2_{\mathrm{hb},1}$ = 1). . . . 5
(*a*) 0th-harmonic . . . 5
(*b*) 1st-harmonic . . . 5
6 Velocity profiles through the center of the lid driven cavity for Re = 1000 . . . 6
(*a*) Vertical velocity profile . . . 6
(*b*) Horizontal velocity profile . . . 6
7 Real part of the density of an acoustic wave with an amplitude of 10 Pa at M = 0.01. . . . 6
8 Streamlines of the zeroth harmonic inside the inter-fin cavity for f = 423.6 Hz, r = 0.0087 m and ND = 6 . . . 7
(*a*) non-preconditioned . . . 7
(*b*) preconditioned . . . 7
9 Work per cycle over the nodal diameter for three different locations of the torsion center for f = 423.6 Hz . . . 7
(*a*) r = −0.069 m . . . 7
(*b*) r = 0.0087 m . . . 7
(*c*) r = 0.122 m . . . 7
10 Comparison of the convergence History of the L1-norm of the residuals for Potsdam's scheme with and without iterative preconditioning with f = 423.6 Hz, r = 0.0087 m and ND = 6 . . . 7
(*a*) 0th harmonic . . . 7
(*b*) 1st harmonic . . . 7
11 Convergence history of the work per cycle for f = 423.6 Hz,r = 0.0087 m and ND = 6 using Potsdam's scheme with and without iterative preconditioning . . . 8

List of Tables